CMS Physics Analysis Summary

Contact: cms-pag-conveners-susy@cern.ch 2014/04/03

Search for direct production of a pair of bottom squarks

The CMS Collaboration

Abstract

This report presents a search for direct production of bottom squark pairs in proton-proton collision events at $\sqrt{s} = 8$ TeV collected by the CMS experiment at the LHC in 2012. The data used correspond to an integrated luminosity of 19.4 fb^{-1}. This search is performed in a final state of two jets, at least one of which is tagged as originating from a b-quark, accompanied by large missing transverse momentum, as well as large transverse mass and contransverse mass calculated from the jets and missing transverse momentum. The observed data in the signal region are consistent with the standard model backgrounds predicted using data control samples. The results are interpreted in terms of a simplified model production of a pair of bottom squarks with each bottom squark decaying to a bottom quark and a weakly interacting stable neutral particle. The production of bottom squarks with mass up to 700 GeV is excluded at 95% confidence level for neutralino masses less than 50 GeV.

1 Introduction

The standard model (SM) has been extremely successful at describing particle physics phenomena. The recently discovered boson with a mass of 125 GeV at the LHC [1, 2] is a prime candidate to be the last particle required in this theory, the Higgs boson. However, the SM suffers from shortcomings such as a mechanism to stabilize the Higgs boson mass against radiative corrections [3–5]. Supersymmetry (SUSY) is an extension to the SM, which relates fermions and bosons. For every known boson (fermion) of the SM, it postulates the existence of a yet unseen fermionic (bosonic) partner. The introduction of these new particles provides solutions to the hierarchy problem. Under the assumption that R-parity is conserved [6–8], a dark matter candidate is also provided in the form of the lightest supersymmetric particle (LSP).

A broad range of searches for light squarks and gluinos [9–15] have been performed by the CMS and ATLAS experiments. SUSY scenarios leading to the production of light top and bottom squarks are well motivated theoretically and have been explored by existing searches [16–27] at the LHC. The motivation arises from naturalness considerations related to protecting the Higgs mass against large loop corrections in the standard model [28]. The first and second generation squarks, in contrast, are not required to be light in such scenarios.

This paper reports on a search for pairs of SUSY particles produced in pp collisions at $\sqrt{s} = 8$ TeV at the LHC using events with a large imbalance in transverse momentum and two energetic jets one or both of which are identified as originating from bottom quarks (b-jets). The data used for this analysis correspond to an integrated luminosity of 19.4 fb^{-1} [29] collected with the CMS experiment [30] during 2012. This final state is motivated by the production of pairs of bottom squarks ($\widetilde{\mathrm{b}}$) where each $\widetilde{\mathrm{b}}$ decays into a bottom quark and a weakly interacting neutral stable particle ($\widetilde{\chi}_1^0$). In a large variety of models $\widetilde{\chi}_1^0$ is the lightest supersymmetric particle and leaves the detector undetected resulting in a characteristic signature of large missing transverse energy ($E_{\mathrm{T}}^{\mathrm{miss}}$), see Figure 1.

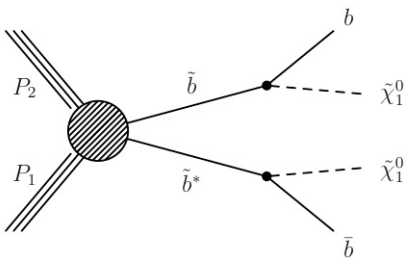

Figure 1: Bottom squark pair production with the bottom squark decaying into a bottom quark and neutralino.

The main background contributions to the search are: $\mathrm{Z}(\nu\bar{\nu})$+jets, an irreducible background; $\mathrm{t\bar{t}}$, single top and $\mathrm{W}(\ell\nu)$+jets events, where a W decays to e or μ (directly or via a τ decay) which survives the lepton veto because it is misidentified, nonisolated or is out of kinematic acceptance, or a τ that decays hadronically and is reconstructed as a jet; and QCD multijet events where semileptonic decays of b-quark jets or mismeasurements of jets can result in large missing transverse momentum.

A brief description of the event reconstruction algorithms is given in Section 2. The simulations of signal and background are described Section 3. The event selection to define the signal region is described in Section 4. Section 5 describes the methods to measure the backgrounds in the search regions using data. Finally, the results are interpreted in Section 6 and concluding remarks are given in Section 7.

2 Detector and Event Reconstruction

The central feature of the CMS detector is a superconducting solenoid, which provides an axial magnetic field of 3.8 T. The bore of the solenoid is instrumented with several particle detection systems. Silicon pixel and strip tracking systems measure charged particle trajectories with full azimuthal (ϕ) coverage and a pseudorapidity acceptance of $|\eta| < 2.5$, where $\eta \equiv -\ln[\tan(\theta/2)]$ and θ is the polar angle with respect to the counterclockwise beam direction. The silicon pixel and strip tracker, the crystal electromagnetic calorimeter (ECAL) and the brass/scintillator hadron calorimeter (HCAL) are contained within the solenoid. Muons are detected in gas-ionization chambers embedded in the steel return yoke. The tracker provides transverse momentum resolution of approximately 1.5% for charged particles with $p_T > 100$ GeV. The ECAL has an energy resolution of better than 0.5 % above 100 GeV. The HCAL combined with the ECAL measures the jet energy with a resolution $\Delta E/E \approx 100\%/\sqrt{E(GeV)} \oplus 5\%$. Events are collected by a two-layer trigger system, based on a hardware filter (L1), followed by a software-based High Level Trigger (HLT). A detailed description of the CMS detector can be found elsewhere [30].

All the final state observables used in this analysis are reconstructed using a particle flow (PF) algorithm [31–33] which combines information from various subdetectors to reconstruct and identify stable particles produced in the collision, namely charged and neutral hadrons, photons, electrons and muons. These particles are then used to calculate the $E_{\mathrm{T}}^{\mathrm{miss}}$ and are clustered to reconstruct jets with the anti-k_{T} algorithm using a distance parameter R=0.5 [34]. The contribution of neutral particles from pileup interactions clustered as jets is subtracted based on the average pileup energy density in an event and the jet area calculated using FastJet tools [35]. The jets are then corrected to take into account the detector response as a function of jet p_{T} and η. These corrections have been derived from Monte Carlo simulated events (MC) and validated using γ+jets and dijet events from collision data. In the end, the jets measured in data are corrected for any residual difference in energy scale between data and MC [36].

Muons are reconstructed by finding compatible track segments in the silicon tracker and the muon detectors [37] and are required to be within $|\eta| < 2.4$. Electron candidates are reconstructed starting from a cluster of energy deposits in the electromagnetic calorimeter that is then matched to the momentum associated with a track in the silicon tracker. Electron candidates are required to have $|\eta| < 1.44$ or $1.56 < |\eta| < 2.5$ to avoid poorly instrumented regions. Muon and electron candidates are required to originate within 2 mm of the beam axis in the transverse plane. A relative isolation parameter is defined as the sum of the p_{T} of the charged hadrons, neutral hadrons, and photon contributions computed in an $\eta - \phi$ cone of radius 0.3 around the lepton direction, divided by the lepton p_{T}. Lepton candidates with relative isolation values below 0.2 are considered isolated.

Jets are identified as b-jets using the "Combined Secondary Vertex (CSV) algorithm" [38]. We use the "loose" and "medium" working point versions of this algorithm. The b-quark identification efficiency for the jets with p_{T} above 70 GeV and $|\eta| < 2.5$ is 80–85% and 46–74% for the loose and medium working points respectively, and the rate for light quarks and gluons being mistagged as b-quark jets for the loose working point and the medium working point are 8–12% and 1–2%, respectively.

3 Monte Carlo event generation

Monte Carlo simulated event samples are used to validate and calibrate the data-driven methods and to calculate the contributions for some small backgrounds. The MADGRAPH5 [39]

program, with up to four additional partons, is used for $t\bar{t}$, $W(\ell\nu)$+jets, $Z(\nu\bar{\nu})$+jets and QCD multijets. The Powheg [40] program is used for single top production and the PYTHIA 6.4.24 [41] program is used to generate diboson samples. Decays of tau leptons are handled by the TAUOLA 27.121.5 [42] program, and the detector response is simulated with the GEANT4 [43] package. All the SM background samples, except for the QCD multijet sample, are normalized to the cross sections calculated at next-to-next-to-leading order (NNLO) [44, 45] or approximate NNLO [46–50] perturbative QCD when available, and otherwise normalized to the cross sections calculated at next-to-leading order (NLO) [51, 52].

The signal samples were generated using the leading order (LO) matrix element event generator MADGRAPH5 with up to 2 additional partons, interfaced with PYTHIA 6.4.24 with tune Z2star [53] for parton showering and hadronization and the CTEQ 6L1 [54] parton distribution functions (PDF), and simulated using parametric simulation. To simulate $\widetilde{b} \to b\widetilde{\chi}_1^0$ events all SUSY particles except $\widetilde{b}$ and $\widetilde{\chi}_1^0$ are assumed to be very heavy and thus do not affect the signal bottom squark production or decay. A grid of signal events is generated as a function of the bottom squark and neutralino masses with 25 GeV and 50 GeV spacings, respectively. The sample covers the range of phase space $(m_{\widetilde{b}}, m_{\widetilde{\chi}_1^0}) = (100 \leq m_{\widetilde{b}} \leq 1000\,\text{GeV}, 1 \leq m_{\widetilde{\chi}_1^0} \leq (m_{\widetilde{b}} - 10)\,\text{GeV})$.

4 Event Selection

We define a signal enriched baseline, which is also used as a loose validation region for comparison of various kinematic distributions in data and MC, using the following selection criteria:

- Exactly two central jets with $p_T > 70$ GeV and $|\eta| < 2.4$. The events are vetoed if they have an additional jet with $p_T > 50$ GeV and $|\eta| < 5.0$.
- One or both of the leading jets are required to be b-jets, using the medium working point.
- Events containing an isolated electron, muon, or track with $p_T > 10$ GeV are rejected to suppress processes such as $t\bar{t}$ and $W(\ell\nu)$+jets.
- $H_T > 250$ GeV, where H_T is the scalar sum of p_T of the two leading jets.
- $E_T^{miss} > 175$ GeV.
- The azimuthal separation between the leading jet (J_1) and sub-leading jet (J_2), $\Delta\phi(J_1, J_2)$, should be less than 2.5 radians to reject QCD dijet events.
- To suppress SM processes such as $t\bar{t}$ and $W(\ell\nu)$+jets, we require the invariant transverse mass of the sub-leading jet and the missing transverse momentum, as defined in Equation 1, to be greater than 200 GeV.

$$M_T(J_2, E_T^{miss}) = \sqrt{[E_T(J_2) - E_T^{miss}]^2 + [\mathbf{p_T}(J_2) - \mathbf{E_T^{miss}}]^2}, \quad (1)$$

  The distribution of $M_T(J_2, E_T^{miss})$ is expected to have a kinematic edge at the mass of the top quark when the jet and E_T^{miss} originate from semileptonic decay of a top quark.

The event samples used to search for the signal are collected with a trigger requiring at least two central jets with $p_T > 50$ GeV and $|\eta| < 2.6$, and $E_T^{miss} > 80$ GeV, reconstructed at trigger level. The trigger efficiency is measured to be larger than 95% for offline selection of $E_T^{miss} > 175$ GeV, and jets with $p_T > 70$ GeV.

We characterize events using the boost-corrected contransverse mass (M_{CT}) [55, 56]. For processes with two identical decays of heavy particles, $\tilde{b} \to J_i \tilde{\chi}_1^0$, the M_{CT} is defined as:

$$\begin{aligned} M_{CT}^2(J_1, J_2) &= [E_T(J_1) + E_T(J_2)]^2 - [\mathbf{p_T}(J_1) - \mathbf{p_T}(J_2)]^2 \\ &= 2p_T(J_1)p_T(J_2)(1 + \cos\Delta\phi(J_1, J_2)), \end{aligned} \quad (2)$$

According to the M_{CT} definition for a given jet p_{T}, events saturate the bound on M_{CT} when two jets point in the same direction in the transverse plane. The $M_{CT}(J_1, J_2)$ distribution is characterized by an endpoint defined by $m_{\tilde{b}}$ and $m_{\tilde{\chi}_1^0}$ which for the topology in question is at $(m(\tilde{b})^2 - m(\tilde{\chi}_1^0)^2)/m(\tilde{b})$.

To obtain sensitivity in multiple regions across the $(m_{\tilde{b}}, m_{\tilde{\chi}_1^0})$ plane, a total of eight exclusive search regions are defined using M_{CT} and the number of b jets ($\mathrm{N_{b-jets}}$), as summarized in Table 1.

Table 1: Definition of eight exclusive search regions.

No. of b-jets	M_{CT}	M_{CT}	M_{CT}	M_{CT}
$\mathrm{N_{b-jets}} = 1$	<250 GeV	250 - 350 GeV	350 - 450 GeV	>450 GeV
$\mathrm{N_{b-jets}} = 2$	<250 GeV	250 - 350 GeV	350 - 450 GeV	>450 GeV

In addition, a set of detector and beam-related cleaning algorithms is applied to remove events with detector noise, which would fake signal-like events with high energy and large transverse imbalance [57, 58].

Comparisons of simulation and data for the key variables, $E_{\mathrm{T}}^{\mathrm{miss}}$ and M_{CT}, in the baseline search regions are shown in Figure 2 for events with $N_{\text{b-jets}}$=1 and $N_{\text{b-jets}}$=2, respectively. The number of events for various SM processes in the signal regions predicted by the simulation are given in Tables 2 and 3. The event yields from simulation are normalized to the integrated luminosity of the data used for this analysis. According to the MC simulation, the contribution from QCD multijet production in the signal region with two b-jets is negligible, so only upper limits on the QCD process are quoted in Table 3. Simulations of the background processes are given in Tables 2 and 3 for illustration only; the background estimates for the search result are obtained from data control regions as described in the next section.

Table 2: Event yields, normalized to the integrated luminosity, from MC simulation after applying all preselection and baseline cuts in the signal region with one b-jet.

	$M_{CT} < 250$ GeV	$250 < M_{CT} < 350$ GeV	$350 < M_{CT} < 450$ GeV	$M_{CT} > 450$ GeV
$Z(\nu\bar{\nu})$+jets	818±12	367±7.8	59±2.8	16±1.5
$W(\ell\nu)$+jets	398±8.4	149±4.9	17±1.5	6.0±0.9
$t\bar{t}$	221±2.5	176±2.2	17± 0.7	2.2±0.2
Single top	33±3.7	13±2.3	0.3±0.3	<0.5
VV	18±0.7	17± 0.6	0.9±0.1	0.3±0.1
ttZ	0.8±0.1	0.5± 0.1	0.2±0.1	<0.04
QCD	12±8.2	6.0± 6.0	< 0.5	<0.5
Total MC	1500±17	729±11	94±3.2	25±1.6

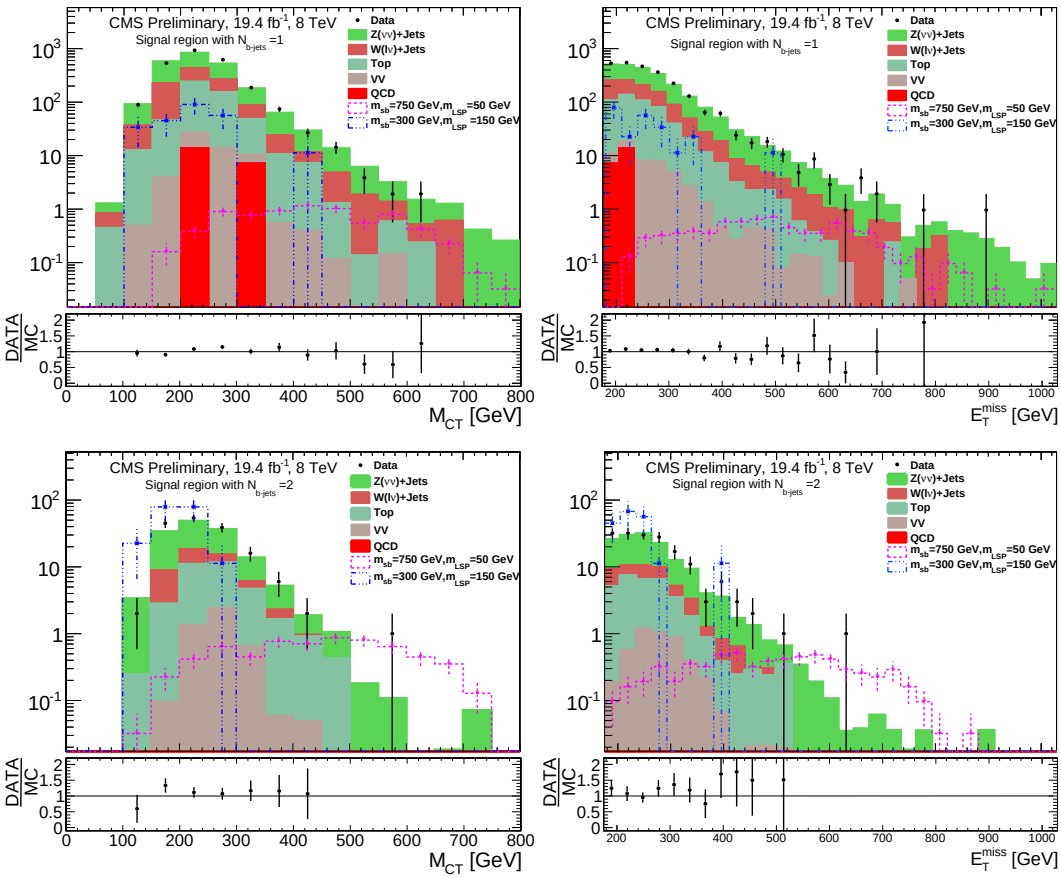

Figure 2: Distributions of M_{CT} and $E_{\mathrm{T}}^{\mathrm{miss}}$ in data and MC for baseline selected events, with $N_{\text{b-jets}}$=1 in the top row and $N_{\text{b-jets}}$=2 in the bottom row. The distributions of M_{CT} and $E_{\mathrm{T}}^{\mathrm{miss}}$ for two signal points, one with $m_{\tilde{b}} = 750$ GeV and LSP mass of 50 GeV and the second point with $m_{\tilde{b}} = 300$ GeV and LSP mass of 150 GeV, are shown by hatched lines.

Table 3: Event yields, normalized to the integrated luminosity, from MC simulation after applying all preselection and baseline cuts in the signal region with two b-jets. According to the MC simulation, the contribution from QCD multijet events in the signal region with two b-jets is negligible, so only the upper limits on the QCD process are quoted here.

	$M_{CT} < 250$ GeV	$250 < M_{CT} < 350$ GeV	$350 < M_{CT} < 450$ GeV	$M_{CT} > 450$ GeV
$Z(\nu\bar{\nu})$+jets	58±3.2	28±2.1	4.8±0.8	1.1±0.3
$W(\ell\nu)$+jets	13±1.4	4.7±1.0	1.0±0.3	< 0.2
$t\bar{t}$	12±0.6	11±0.5	1.8± 0.2	0.3±0.1
Single t	1.3±0.7	2.2±1.1	<0.5	<0.5
VV	1.5±0.1	3.2± 0.2	0.1±0.0	<0.1
ttZ	0.3±0.1	0.2± 0.1	<0.04	<0.04
QCD	<0.5	<0.5	< 0.5	<0.5
Total MC	86±3.6	49±2.5	7.7±0.8	1.4±0.4

5 Estimation of Standard Model Backgrounds

In all the search regions, the $Z(\nu\bar{\nu})$+jets process is the dominant background followed by the contributions of $W(\ell\nu)$+jets and $t\bar{t}$ processes. These backgrounds, as well as the contribution from QCD multijet production, are determined using the data. A single muon control sample selected from data is used to estimate the numbers of $Z(\nu\bar{\nu})$+jets, $t\bar{t}$ and $W(\ell\nu)$+jets background events in the signal regions. The single muon events used to measure $Z(\nu\bar{\nu})$+jets background are required to not have any b-jets to select a $W(\ell\nu)$+jets enriched sample. The $W(\ell\nu)$+jets, single top and $t\bar{t}$ backgrounds are measured using the events selected with the signal definition except that events are required to have exactly one isolated muon. The contribution of QCD multijet events is negligible in all the search bins as suggested by the MC predictions but it is also estimated directly from data control regions. The contribution of diboson and Drell-Yan processes in the signal regions is less than 3% and is estimated from simulation assuming a 50% systematic uncertainty. These contributions are listed as "rare processes" in Table 10.

Jet, lepton, b-jet multiplicity and kinematic requirements for the signal regions and all control samples are summarized in Table 4.

5.1 Estimation of $Z(\nu\bar{\nu})$+jets Background

The contribution of $Z(\nu\bar{\nu})$+jets events is estimated using $W(\mu\nu)$+jets events as the two processes have similar kinematic characteristics. To mimic the signature of neutrinos from decays of the Z boson, the muon $\vec{p}_{\mathrm{T}}$ is added to $\mathbf{E}_{\mathrm{T}}^{\mathrm{miss}}$ to define a "Modified $\mathbf{E}_{\mathrm{T}}^{\mathrm{miss}}$", which is then used to compute the various event selection variables.

This background is estimated from a data sample of single muon events selected from isolated muon triggers by requiring exactly one isolated muon with $p_{\mathrm{T}} > 30$ GeV and $|\eta| < 2.1$. The event is vetoed if there is an additional muon candidate in the event such that the invariant mass formed by the two muons is within 25 GeV of the mass of the Z boson. The muon is required to be separated from the closest jet in the event by $\Delta R = \sqrt{(\Delta\eta)^2 + (\Delta\phi)^2} > 0.3$. The events should satisfy the same criteria for jets as used for the signal regions except that the events with an identified b-jet using the loose working point are rejected to minimize the contribution of $t\bar{t}$ or single top events. Selection thresholds for the Modified $E_{\mathrm{T}}^{\mathrm{miss}}$, H_{T} and $M_T(J_2, \mathrm{Modified}E_{\mathrm{T}}^{\mathrm{miss}})$ are the same as those used to define the signal regions. The $\Delta\phi(J_1, J_2)$ requirement is ignored in the definition of the single muon control sample. All the requirements that are applied to

Table 4: Jet, lepton, b-jet, the CSV working points (Loose or Medium WP) and kinematic requirements for the signal regions and all control samples.

Requirements			
Jet	Lepton	b-jet	Kinematics
Signal region			
Two Central Jets Veto 3rdjet,p_T >50 GeV	lepton(e and μ) veto Isolated Track veto	$N_{\text{b-jets}}$=1,2 Medium WP	$M_T(J_2, E_T^{miss}) > 200$ GeV, H_T> 250 GeV $E_T^{miss} > 175$ GeV and $\Delta\phi(J_1, J_2) < 2.5$
W($\mu\nu$)+jets control sample			
Two Central Jets Veto 3rdjet,p_T >50 GeV	One tight μ, $\|\eta\|$ <2.1 p_T> 30 GeV	$N_{\text{b-jets}}$=0 Loose WP	$M_T(J_2, E_T^{miss}) > 200$ GeV, H_T> 250 GeV Modified $E_T^{miss} > 175$ GeV
μ+jets control sample			
Two Central Jets Veto 3rdjet,p_T >50 GeV	One tight μ, $\|\eta\|$ <2.1 p_T> 10 GeV	$N_{\text{b-jets}}$=1,2 Loose WP	$M_T(J_2, E_T^{miss}) > 200$ GeV, H_T> 250 GeV $E_T^{miss} > 175$ GeV
QCD control samples			
Two Central Jets Veto 3rdjet,p_T >50 GeV	lepton(e and μ) veto Isolated Track veto	$N_{\text{b-jets}}$=0,1,2 Medium WP	H_T> 250 GeV $E_T^{miss} > 175$ GeV and $\Delta\phi(J_1, J_2) > 2.5$

define the W($\mu\nu$)+jets control sample are summarized in Table 4. Figure 3 compares the M_{CT} and Modified E_T^{miss} distributions for simulated and data events in the control sample. The data is below the MC by up to 50% at high M_{CT}; however our use of the control sample data for background predictions avoids the effects of such MC mismodelling.

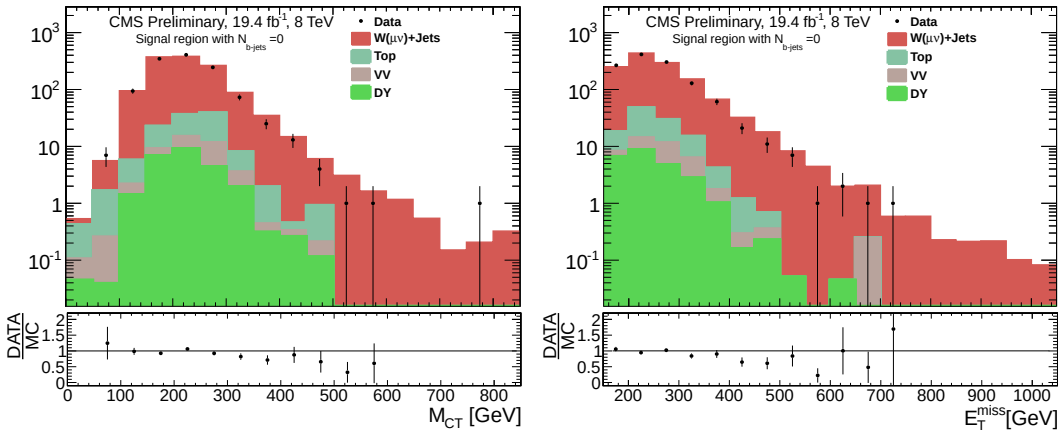

Figure 3: Comparison of simulation and data for the (a) M_{CT} and (b) E_T^{miss} distribution in the single muon control sample used to estimate $Z(\nu\bar{\nu})$+jets background. The distributions are shown after applying all cuts in the control sample.

Starting from the single muon control sample as described above, the prediction of the number of $Z(\nu\bar{\nu})$+jets events can be written as:

$$N(Z \to \nu\bar{\nu}) = \frac{N^{obs} - N^{Non-W}}{\epsilon_\mu \epsilon_{HLT}} R\left(\frac{Z \to \nu\bar{\nu}}{W \to \mu\nu}\right). \quad (3)$$

While Equation 3 is defined for each of the eight search regions, the $N^{obs} - N^{Non-W}$ is the same for both b-jet multiplicities for a given M_{CT} range. The ϵ_μ is the correction for differences in

Table 5: Predicted event yields for $Z(\nu\bar{\nu})$+jets background in the M_{CT} and b-jet multiplicity bins using the method explained in the text. These numbers are comparable with the expected event yields from simulation for the $Z(\nu\bar{\nu})$+jets background in Tables 2 and 3.

	M_{CT} <250 GeV	250< M_{CT} <350 GeV	350< M_{CT} <450 GeV	M_{CT} > 450 GeV
$Z(\nu\bar{\nu})$+jets $N_{\text{b-jets}}$=1	848±12± 79	339±8.1±52	48±3.0±6.0	8.1±1.6±1.7
$Z(\nu\bar{\nu})$+jets $N_{\text{b-jets}}$=2	60±3.4±7.1	28±2.4±3.8	3.9±0.9±1.0	0.7±0.6±0.6

the muon isolation and identification efficiencies for data and MC, ϵ_{HLT} is the trigger efficiency, N^{obs} is the number of events passing the W($\rightarrow \mu\nu$) selection and N^{Non-W} represents the number of single top, $t\bar{t}$, Drell-Yan, and diboson events. Finally, R($\frac{Z\rightarrow\nu\bar{\nu}}{W\rightarrow\mu\nu}$) is the ratio of number of $Z(\nu\bar{\nu})$+jets and W($\mu\nu$)+jets events expected from simulation in a given search bin defined by M_{CT} and $N_{\text{b-jets}}$. R includes the cross sections for W($\mu\nu$)+light flavor-jets and $Z(\nu\bar{\nu})$+heavy flavor-jets processes, acceptance effects for detecting the muon, and the branching fractions for the W and Z bosons.

The resulting predicted numbers of $Z(\nu\bar{\nu})$+jets events for each M_{CT} bin are shown in Table 5 for events with one and two b-jets along with the statistical and total systematic uncertainties.

We evaluate systematic uncertainties on the $Z(\nu\bar{\nu})$+jets background prediction resulting from the method, simulation mismodelling and misidentifications, as described below.

- **Theoretical uncertainties on R**: We consider theoretical uncertainties on the production of W($\ell\nu$)+jets and $Z(\nu\bar{\nu})$+jets processes from higher-order QCD corrections, the PDF uncertainties and higher-order electroweak corrections. The total theoretical QCD uncertainty is expected to be less than 5% and the uncertainty from the choice of the PDFs is negligible as it almost completely cancels in the ratio W/Z as a function of boson p_{T}. The higher-order electroweak corrections are similar for the W and Z production and largely cancel in the cross section ratios [59].
- **Cross section for W and Z production in association with b jets**: Another source of uncertainty on the ratio R can arise from the difference in production of Z bosons in association with one or two b-jets in data and MC simulation. An overall conservative systematic uncertainty is assigned on the $Z(\nu\bar{\nu})$+b-jets cross section. This uncertainty is obtained from the statistical precision of the Data/MC ratio for the $Z \rightarrow \mu\bar{\mu}$ events with at least one b-jet. This is measured to be about 5% with the data covering M_{CT} values up to 250 GeV; we apply that value for all M_{CT} regions.
- **Statistical uncertainty on R**($\frac{Z\rightarrow\nu\bar{\nu}}{W\rightarrow\mu\nu}$): The statistical uncertainties of the simulated $Z(\nu\bar{\nu})$+jets and W($\ell\nu$)+jets samples are propagated for each search bin.
- **Contamination from other SM processes**: The W($\mu\nu$)+jets event sample selected from data also has contributions from Drell-Yan, diboson, and $t\bar{t}$ and single top processes, as indicated by N^{Non-W} in Equation 3. As mentioned earlier, events with a reconstructed b-jet are vetoed and this requirement efficiently rejects most of the $t\bar{t}$ events. The total contribution from all the processes other than W($\mu\nu$)+jets production is less than $(10-12)$% in the various M_{CT} bins. We use the MC event yields of these processes and subtract them from the number of events in the single muon data control sample. We vary the production cross section of these processes up and down by 50% to assign an additional systematic uncertainty on the number of

$Z(\nu\bar{\nu})$+jets predicted from the data. The total uncertainty is less than 9% for one b-jet and 8% for two b-jets for the various search regions.

- **Non-Closure**: This uncertainty is motivated to account for any lack of closure which may be hidden by the statistical precision of the method due to the size of the MC sample. The statistical uncertainty on the closure test performed on the MC dataset is used as an additional uncertainty on the number of $Z(\nu\bar{\nu})$+jets events predicted from data. The systematic uncertainty due to closure tests varies from 2 to 13% for $N_{\text{b-jets}}$=1 and from 6 to 30% for $N_{\text{b-jets}}$=2.

The total uncertainties on the predicted number of $Z(\nu\bar{\nu})$+jets events in the eight search regions are summarized in Table 6. The table also provides a detailed breakdown of the various components of the systematic with respect to the $Z(\nu\bar{\nu})$+jets background in a given search region.

Table 6: Systematic uncertainties on the predicted numbers of $Z(\nu\bar{\nu})$+jets events for various search regions.

	M_{CT} <250 GeV $N_{\text{b-jets}}$=1	250< M_{CT} <350 GeV $N_{\text{b-jets}}$=1	350< M_{CT} <450 GeV $N_{\text{b-jets}}$=1	M_{CT} > 450 GeV $N_{\text{b-jets}}$=1
R($\frac{Z\to\nu\bar{\nu}}{W\to\mu\nu}$)	±0.3%	±3.2%	±2.1%	±10.0%
DY+VV+Top	±4.2%	±8.6%	±3.3%	±7.4%
ϵ_μ(Iso+ID)	±3.4%	±6.1%	±5.6%	±9.5%
ϵ_{HLT}	±1.2%	±2.6%	±2.5%	±2.5%
Theroretical Unc.	±5.2%	±5.2%	±5.2%	±5.0%
Non-Closure	±2%	±8%	±7%	±13%
(Z+b) X-section	±5.3%	±5.3%	±5.3%	±5.3%
Total Sys.Unc	±9.3%	±15.3%	±12.5%	±21.7%
	M_{CT} <250 GeV $N_{\text{b-jets}}$=2	250< M_{CT} <350 GeV $N_{\text{b-jets}}$=2	350< M_{CT} <450 GeV $N_{\text{b-jets}}$=2	M_{CT} > 450 GeV $N_{\text{b-jets}}$=2
R($\frac{Z\to\nu\bar{\nu}}{W\to\mu\nu}$)	±1.3%	±2.5%	±18%	±85.7%
DY+VV+Top	±4.3%	±5.0%	±2.6%	±7.1%
ϵ_μ(Iso+ID)	±5.7%	±6.1%	±10.2%	±5.7%
ϵ_{HLT}	±2.3%	±2.5%	±2.6%	±2.8%
Theroretical Unc.	±5.2%	±4.3%	±5.0%	±4.3%
Non-Closure	±6%	±8%	±17%	±30%
(Z+bb) X-section	±5.3%	±5.3%	±5.3%	±5.3%
Total Sys.Unc	±11.9%	±13.5%	±26.8%	±91.5%

5.2 Estimation of W($\ell\nu$) background

The background due to $t\bar{t}$, single top and W($\ell\nu$)+jets processes is estimated using events collected with the same trigger and selection as for the search regions, except for requiring rather than vetoing events with a single muon. In addition, the requirement on $\Delta\phi(J_1, J_2) < 2.5$ is not used. To increase the control sample statistics, the loose b-jet identification working point is used instead of the medium working point. A summary of the cuts is provided in Table 4. M_{CT} and $E_{\text{T}}^{\text{miss}}$ distributions comparing data and simulation in the control samples with $N_{\text{b-jets}}$=1 or $N_{\text{b-jets}}$=2 are shown in the top and bottom rows of Figure 4, respectively.

Starting from the numbers of single muon events in a search region, the numbers of $t\bar{t}$, single top and W($\ell\nu$)+jets are predicted according to Equation 4 using a translation factor obtained

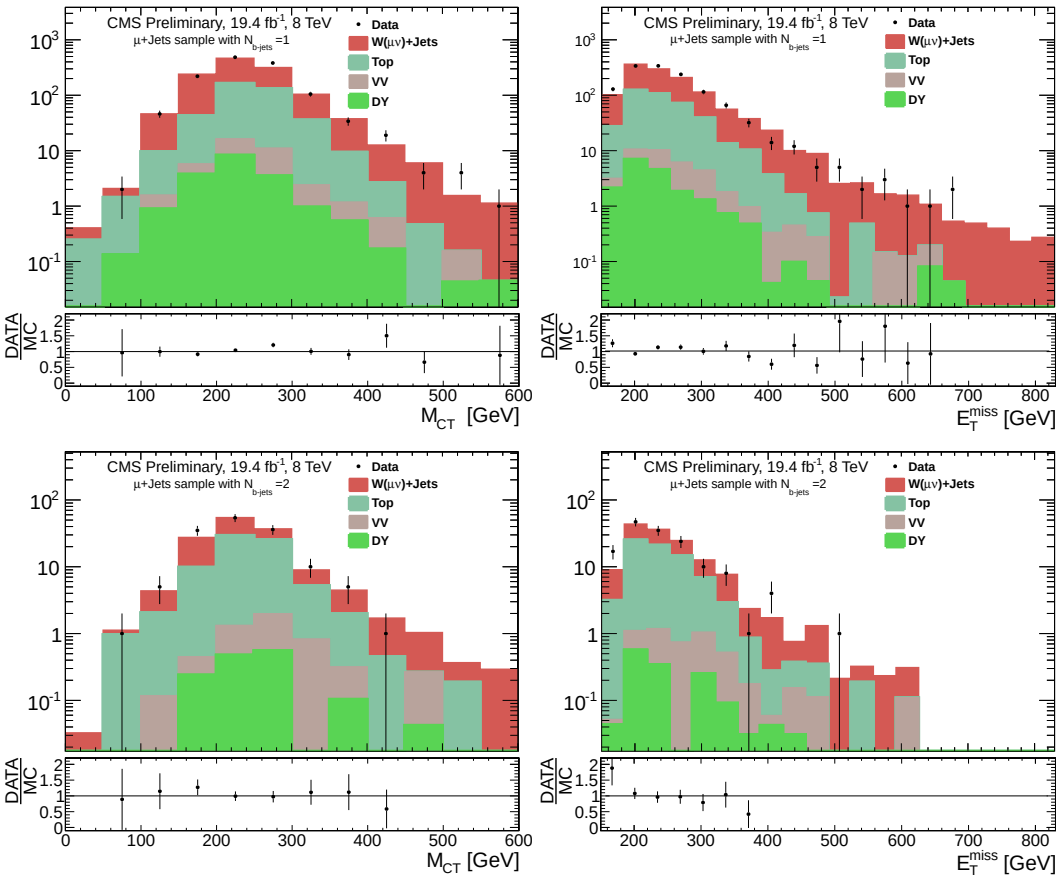

Figure 4: Distributions of M_{CT} and $E_{\mathrm{T}}^{\mathrm{miss}}$ for data versus simulation for the events with exactly one b-jet (top row) and exactly two b-jets (bottom row). The distributions are shown after applying all cuts in the control sample.

from MC simulated events.

$$N^{Pred}_{Signal}(M_{CT}, N_{\text{b-jets}}) = N^{obs}_{Control}(M_{CT}, N_{\text{b-jets}}) \times (\frac{N^{MC}_{Signal}}{N^{MC}_{Control}})(M_{CT}, N_{\text{b-jets}}), \quad (4)$$

where $N^{MC}_{Signal}(M_{CT}, N_{\text{b-jets}})$ are the numbers of W($\ell\nu$)+jets, $t\bar{t}$ and single top in a given $(M_{CT}, N_{\text{b-jets}})$ region, and $N^{MC}_{Control}(M_{CT}, N_{\text{b-jets}})$ are the numbers of events in the single muon control sample due to the processes W+jets, $t\bar{t}$, single top, diboson and Drell-Yan obtained using simulated samples. The $N^{obs}_{Control}(M_{CT}, N_{\text{b-jets}})$ are the numbers of events selected in the control region for data. The predicted numbers of $t\bar{t}$, single top and W($\ell\nu$)+jets events in the various search regions are given in Table 7, along with the statistical and total systematic uncertainties.

Table 7: Predicted event yields for W+jets, $t\bar{t}$ and single top from data for all search regions. The errors on the predicted numbers are the statistical and the total systematic uncertainties.

	$M_{CT} < 250$ GeV	$250 < M_{CT} < 350$ GeV	$350 < M_{CT} < 450$ GeV	$M_{CT} > 450$ GeV
Top+W($\ell\nu$)+jets $N_{\text{b-jets}}$=1	645±24±57	381±17±38	36±4.9±5.7	7.8 ±2.6±2.0
Top+W($\ell\nu$)+jets $N_{\text{b-jets}}$=2	29±2.9±5.5	17±2.5±3.3	2.4±0.9±0.6	0.2±0.2

Since the data and simulation control and signal samples are defined to be kinematically similar, most of the uncertainties in the mismodelling of event kinematics in simulation or instrumental effects observed in data are expected to largely cancel in the ratio of the number of events used to construct the translation factors. Possible sources of the remaining uncertainties on the predicted numbers of $t\bar{t}$, single top and W($\ell\nu$)+jets events in the signal regions are described next.

The $t\bar{t}$ and W($\ell\nu$)+jets composition changes in different kinematic regions or different b-jet multiplicity selections. For example, in various M_{CT} regions, $t\bar{t}$+jets events constitute 25–50% of the control sample with one b-jet and 50–100% for the control sample with two b-jets. Therefore, the translation factors obtained from simulated samples are validated using data. To probe the sensitivity of the translation factors to the admixture of $t\bar{t}$ and W($\ell\nu$)+jets processes, a muon control sample with one b-jet is used to predict event yields in the single muon control sample with two b-jets using the translation factors obtained from MC. The predicted numbers of events are then compared with the numbers of events with two b-jets observed in data. Another source of uncertainty on the translation factors results from the differences in modeling of lepton isolation and the isolated track veto in the data and the MC. To probe this effect, the numbers of events with exactly one muon are predicted starting from a control sample with an isolated track and no isolated muon or electron with $p_T > 10$ GeV using translation factor derived from MC. The average weighted error of the two tests results in 8–20% uncertainty on the predicted $t\bar{t}$ and W($\ell\nu$)+jets background in various signal regions. Uncertainties of 3–15% and 8–42% are assigned to the predicted background due to the statistics of the MC samples used for events with one and two b-jets respectively. The uncertainties on correcting efficiencies for identifying b-jets results in 2- 20% uncertainties on the final prediction. The uncertainty due to the contributions of dibosons and other rare processes is less than 2% across all the search bins. Table 8 provides a detailed breakdown of the various components of the systematic uncertainties with respect to the background in a given search region.

Table 8: The uncertainties on the predicted top and W($\ell\nu$)+jets background are shown for all M_{CT} and $N_{\text{b-jets}}$ bins. TF stands for the translation factor.

	M_{CT} <250 GeV $N_{\text{b-jets}}$=1	250< M_{CT} <350 GeV $N_{\text{b-jets}}$=1	350< M_{CT} <450 GeV $N_{\text{b-jets}}$=1	M_{CT} > 450 GeV $N_{\text{b-jets}}$=1
TF (Stat)	±2.6%	±2.4%	±6.6%	±14.6%
TF (Sys)	±8.0%	±9.0%	±13.7%	±20.0%
SF(b-tag)	±2.8%	±3.7%	±3.6%	±8.8%
DY+VV Cont	±1.5%	±1.6%	±1.6%	±1.1%
Total Sys.Unc	±8.9%	±10.1%	±15.7%	±26.3%
	M_{CT} <250 GeV $N_{\text{b-jets}}$=2	250< M_{CT} <350 GeV $N_{\text{b-jets}}$=2	350< M_{CT} <450 GeV $N_{\text{b-jets}}$=2	M_{CT} > 450 GeV $N_{\text{b-jets}}$=2
TF (Stat)	±8.1%	±9.8%	±20.7%	±41.8%
TF (Sys)	±8.0%	±9.0%	±13.7%	±20.0%
SF(b-tag)	±14.9%	±13.7%	±6.1%	±11.9%
DY+VV Cont	±1.1%	±2.9%	±3.03%	±8.0%
Total Sys.Unc	±18.8%	±19.3%	±25.7%	±48.5%

5.3 Estimation of QCD Background

Due to the $\Delta\phi$ requirement the QCD contribution is expected to be at the less than a percent level for all the search bins. An estimate of this contribution is made by measuring the number of QCD multijet events in a QCD enriched control region and scaling this number by a translation factor. The control regions are identical to the search regions except that the $\Delta\phi$ requirement is inverted. The translation factor is found in a sideband region by measuring the ratio between the number of QCD multijet events with the standard and inverted $\Delta\phi$ requirements as determined from data.

To define the sideband region we use the observation that for the QCD events $\Delta\phi$ is uncorrelated with the CSV discriminator of the leading jet (CSV1) and sub-leading jet (CSV2). The ratio between the number of QCD multijet events with the standard $\Delta\phi$ requirement to the number of QCD events in the inverted $\Delta\phi$ region remains constant as a function of the sum of the CSV discriminators for the two leading jets ($\text{CSV}_{J_1J_2}$= CSV1+CSV2). The sideband is selected by a $0.24 < \text{CSV}_{J_1J_2} < 0.68$ requirement.

Since the sideband with $\Delta\phi(J_1, J_2) < 2.5$ is dominated by Z($\nu\bar{\nu}$)+jets, $\mathrm{t\bar{t}}$ and W($\ell\nu$)+jets events, we try to select the QCD events using the feature of the QCD events that pass the $\Delta\phi$ requirement. The QCD events that survive in the sideband with the standard $\Delta\phi$ requirement are usually due to under-measurement of one of the two leading jets as a third leading jet. In these events $E_{\text{T}}^{\text{miss}}$ is closely aligned with the direction of third leading jet (J_3), so these events can then be selected using a $\Delta\phi(J_3, E_{\text{T}}^{\text{miss}}) < 0.3$ requirement. To estimate the number of QCD multijet events in the sideband with the standard $\Delta\phi$ requirement, we subtract the contribution of non-QCD processes from the observed events and in order to take into account any data and MC discrepancy, the numbers of non-QCD events are scaled by a data/MC correction factor which is determined in a QCD free region. The resulting predictions for the numbers of QCD events in each search region using the method explained above are shown in Table 9. The statistical uncertainties on the predicted numbers of QCD background events, originating from the statistics of the numbers of observed events in the control samples and the statistical uncertainty on the numbers of non-QCD events, are propagated as a systematic uncertainty on the QCD prediction.

Table 9: QCD background predictions in the signal regions.

	$M_{CT} < 250$ GeV	$250 < M_{CT} < 350$ GeV	$350 < M_{CT} < 450$ GeV	$M_{CT} > 450$ GeV
QCD $N_{\text{b-jets}}$=1	25±9.4±5.2	16±7.4±2.8	$1.0^{+1.2}_{-1.0}$	$1.0^{+1.2}_{-1.0}$
QCD $N_{\text{b-jets}}$=2	1.9±0.7±0.4	1.2±0.8±0.2	$0.1^{+0.1}_{-0.1}$	$0.1^{+0.1}_{-0.1}$

6 Results and Interpretation

Table 10 summarizes the background predictions as described in Section 5, and compares them to the yields observed in the eight signal regions; the visual representation is shown in Figure 5. The data are consistent with the backgrounds expected from the SM processes. Therefore, we proceed to set limits on sparticle masses; the result is interpreted in simplified models (SMS) [60–63]. The simplified models are formulated as an effective Lagrangian describing a small number of new particles and their interactions with arbitrary correlation. The masses of the primary particles and their decay products are free parameters. This makes it possible to study the SUSY or SUSY-like parameter space in a generic way. Although the nomenclature of particles is phrased in terms of superpartner names, the results are applicable to any theoretical model which would result in a given final state topology. We consider an SMS scenario, known as T2bb, in which sbottom squarks are produced in pairs, with each decaying to a bottom quark and an invisible massive particle.

Table 10: Predicted event yields for the different background contributions are compared with data in each search region. The uncertainties on predicted background yields are the quadratic sum of the systematic and statistical uncertainties.

	M_{CT} <250 GeV $N_{\text{b-jets}}$=1	250< M_{CT} <350 GeV $N_{\text{b-jets}}$=1	350< M_{CT} <450 GeV $N_{\text{b-jets}}$=1	$M_{CT} > 450$ GeV $N_{\text{b-jets}}$=1
$Z(\nu\bar{\nu})$+jets	848±12±79	339±8.1±52	48±3.0±6.0	8.1±1.6±1.7
Top+W$(\ell\nu)$+jets	645±24±57	381±17±38	36±4.9±5.7	7.8 ±2.6±2.0
QCD	25±9.4±5.2	16±7.4±2.8	$1.0^{+1.2}_{-1.0}$	$1.0^{+1.2}_{-1.0}$
Rare processes	18 ± 9.2	18±8.9	1.1±0.5	0.3±0.1
Total Background	1536±102	754±68	86±10	17 ±4.1
Data	1556	807	101	23
	M_{CT} <250 GeV $N_{\text{b-jets}}$=2	250< M_{CT} <350 GeV $N_{\text{b-jets}}$=2	350< M_{CT} <450 GeV $N_{\text{b-jets}}$=2	$M_{CT} > 450$ GeV $N_{\text{b-jets}}$=2
$Z(\nu\bar{\nu})$+jets	60±3.4±7.1	28±2.4±3.8	3.9±0.9±1.0	0.7±0.6±0.6
Top+W$(\ell\nu)$+jets	29±2.9±5.5	17±2.5±3.3	2.4±0.9±0.6	0.2±0.2
QCD	1.9±0.7±0.4	1.2±0.8±0.2	0.1±0.1	0.1±0.1
Rare processes	1.8 ± 0.9	3.4±1.7	0.1±0.1	0.1±0.1
Total Background	93±10	50±6.4	6.5±1.7	1.0 ±0.9
Data	101	55	8	1

We evaluate 95% confidence level (CL) exclusion limits on the signal production cross section using the CLs method, which assumes a fully frequentist approach. We use the standard limit setting tools from the ROOSTATS package to perform the CLs calculation [64, 65].

The eight signal bins in M_{CT} and b-jet multiplicity are used as separate statistically independent

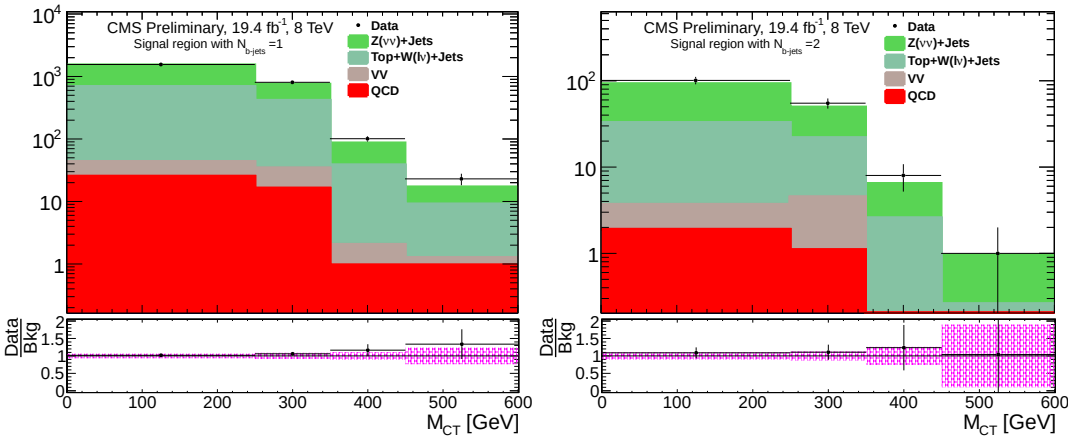

Figure 5: Comparison of data and predicted backgrounds in the various M_{CT} and b-jet multiplicity bins. The hatched lines represent the total uncerainties on the total numbers of predicted events.

channels in the limit calculation, and the correlations among the systematic uncertainties in different bins are taken into account.

Uncertainties on the signal yield predictions are accounted for as follows: the luminosity determination (2.6%) [66], the signal acceptance and efficiency arising from the jet energy corrections and jet energy resolution (5%), parton distribution functions (PDF) of the proton, trigger inefficiency (5%), the event cleaning procedure (2.5%) [57, 58], modelling of initial or final state radiation (1%-20%) [22] and b-tagging data and MC scale factors (2%-25%). The acceptance of the signal is obtained after re-weighting the signal events with both the b-tagging scale factors and corrections for the initial state radiation [22] in signal MC generation to match that measured in data.

Figure 6 shows the expected and observed 95% confidence level upper limits on the bottom squark cross sections in the $(m_{LSP}, m_{\tilde{b}})$ plane. The cross sections are determined at NLO in the strong coupling constant and include the resummation of soft gluon emission at the accuracy of next-to-leading-log (NLL) level [67–71]. We choose to depict the one standard deviation experimental (theoretical) error around the expected (observed) exclusion curve. The theoretical error is based on changing the renormalization and factorization scales by a factor of 2 and using the PDF4LHC recommendation [72] for the PDF uncertainty to illustrate the sensitivity of the exclusion to the signal cross section uncertainty. For small LSP masses, the observed limit less one standard deviation of the theory uncertainty excludes bottom squark masses below 700 GeV at 95% confidence level.

7 Conclusions

A search for pair production of bottom squarks is reported, based on a data sample of pp collisions collected with the CMS detector at $\sqrt{s} = 8$ TeV, corresponding to an integrated luminosity of 19.4 fb^{-1}. Final states with two jets and significant $E_{\mathrm{T}}^{\mathrm{miss}}$ have been analysed. The search has been performed in exclusive binned signal regions defined by the number of jets identified to originate from a b-quark and the contransverse mass, M_{CT}. The standard model backgrounds per bin have been estimated from μ + jets samples, with and without a b-tag. We observe no excess above the SM predictions. Exclusion limits are set at the 95% CL on the simplified model production of a pair of bottom squarks with each bottom squark decaying to a bottom quark

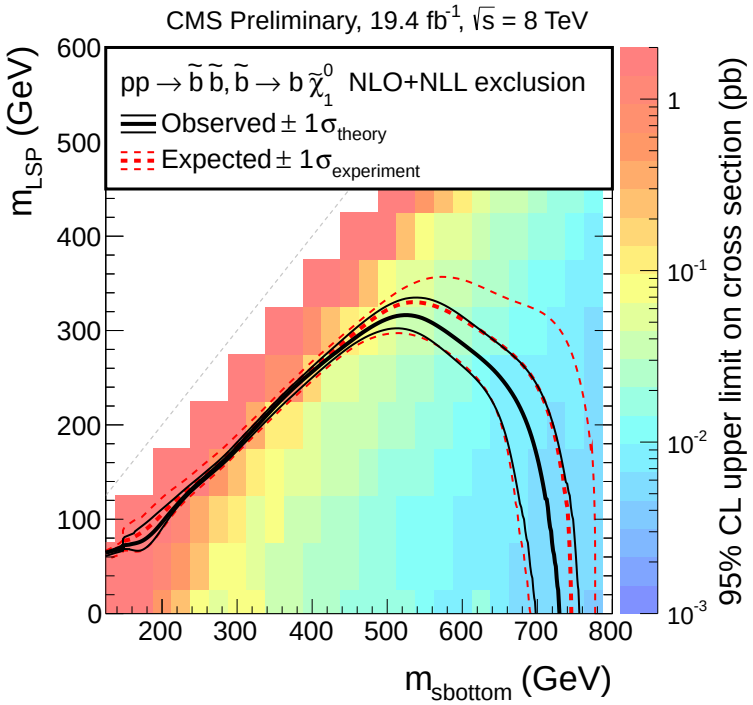

Figure 6: Combined 95% CL exclusion limits for bottom squark pair production. The plot shows the expected limit as a red dashed line. The observed limit is shown as a black solid line. The dashed red (solid black) lines represent the expected (observed) exclusion contours at 95% CL. The total experimental uncertainty is shown around the expected limit contour as dashed red lines, and the theoretical uncertainty is shown around the observed limit contour as thin black lines.

and the lightest neutralino. The production of bottom squarks with mass up to 700 GeV is excluded at 95% confidence level for neutralino masses less than 50 GeV.

References

[1] CMS Collaboration, "Observation of a new boson at a mass of 125 GeV with the CMS experiment at the LHC", *Phys. Lett. B* **716** (2012) doi:10.1016/j.physletb.2012.08.021.

[2] ATLAS Collaboration, "Observation of a new particle in the search for the Standard Model Higgs boson with the ATLAS detector at the LHC", *Phys. Lett. B* **716** (2012) doi:10.1016/j.physletb.2012.08.020.

[3] S. Weinberg, "Implications of Dynamical Symmetry Breaking", *Phys. Rev. D* **13** (1976) 974–996.

[4] E. Gildener, "Gauge Symmetry Hierarchies", *Phys. Rev. D* **14** (1976) 1667.

[5] S. Weinberg, "Implications of Dynamical Symmetry Breaking, An Addendum", *Phys. Rev. D* **19** (1979) 1277–1280.

[6] P. Fayet, "Supersymmetry and Weak, Electromagnetic and Strong Interactions", *Phys. Lett. B* **64** (1976) 159.

[7] P. Fayet, "Spontaneously Broken Supersymmetric Theories of Weak, Electromagnetic and Strong Interactions", *Phys. Lett. B* **69** (1977) 489.

[8] G. Farrar and et al, "Phenomenology of the Production, Decay, and Detection of New Hadronic States Associated with Supersymmetry", *Phys. Lett. B* **76** (1978) 575.

[9] CMS Collaboration, "Search for New Physics with Jets and Missing Transverse Momentum in pp collisions at $\sqrt{s} = 7$ TeV", *JHEP* **08** (2011) 155, doi:10.1007/JHEP08(2011)155, arXiv:1106.4503.

[10] CMS Collaboration, "Inclusive search for squarks and gluinos in pp collisions at $\sqrt{s} = 7$ TeV", *Phys. Rev. D* **85** (2012) 012004, doi:10.1103/PhysRevD.85.012004, arXiv:1107.1279.

[11] CMS Collaboration, "Search for supersymmetry in hadronic final states using M_{T2} in pp collisions at $\sqrt{s} = 7$ TeV", *JHEP* **10** (2012) 018, doi:10.1007/JHEP10(2012)018, arXiv:1207.1798.

[12] CMS Collaboration, "Search for gluino mediated bottom- and top-squark production in multijet final states in pp collisions at 8 TeV", *Phys. Lett. B* **725** (2013) 243, doi:10.1016/j.physletb.2013.06.058, arXiv:1305.2390.

[13] ATLAS Collaboration, "Search for squarks and gluinos with the ATLAS detector in final states with jets and missing transverse momentum using 4.7 fb^{-1} of $\sqrt{s} = 7$ TeV proton-proton collision data", *Phys. Rev. D* **87** (2013) 012008, doi:10.1103/PhysRevD.87.012008, arXiv:1208.0949.

[14] ATLAS Collaboration, "Hunt for new phenomena using large jet multiplicities and missing transverse momentum with ATLAS in 4.7 fb^{-1} of $\sqrt{s} = 7$ proton-proton collisions", *JHEP* **07** (2012) 167, doi:10.1007/JHEP07(2012)167, arXiv:1206.1760.

[15] ATLAS Collaboration, "Search for new phenomena in final states with large jet multiplicities and missing transverse momentum at $\sqrt{(s)} = 8$ TeV proton-proton collisions using the ATLAS experiment", *JHEP* **10** (2013) 130, doi:10.1007/JHEP10(2013)130.

[16] ATLAS Collaboration, "Search for scalar bottom pair production with the ATLAS detector in pp collisions at sqrt(s) = 7 TeV", *Phys. Rev. Lett.* **108** (2012) 181802, doi:10.1103/PhysRevLett.108.181802.

[17] ATLAS Collaboration, "Search for light top squark pair production in final states with leptons and b-jets with the ATLAS detector in $\sqrt{s} = 7$ TeV proton-proton collisions", *Phys. Lett. B* **720** (2013) 13–31, doi:10.1016/j.physletb.2013.01.049.

[18] ATLAS Collaboration, "Search for direct third-generation squark pair production in final states with missing transverse momentum and two b-jets in $\sqrt{s} = 8$ TeV pp collisions with the ATLAS detector", *JHEP* **10** (2013) 189, doi:10.1007/JHEP10(2013)189, arXiv:1308.2631.

[19] ATLAS Collaboration Collaboration, "Search for a heavy top-quark partner in final states with two leptons with the ATLAS detector at the LHC", *JHEP* **1211** (2012) 094, doi:10.1007/JHEP11(2012)094, arXiv:1209.4186.

[20] CMS Collaboration, "Search for supersymmetry in final states with missing transverse energy and 0, 1, 2, or $\geq$3 b-quark jets in 7 TeV pp collisions using the variable α_{T}", *JHEP* **01** (2013) 077, doi:10.1007/JHEP01(2013)077, arXiv:1210.8115.

[21] CMS Collaboration, "Search for supersymmetry in hadronic final states with missing transverse energy using the variables AlphaT and b-quark multiplicity in pp collisions at 8 TeV", *EPJC* **73** (2013) 2568, doi:10.1140/epjc/s10052-013-2568-6, arXiv:1303.2985.

[22] CMS Collaboration, "Search for top-squark pair production in the single-lepton final state in pp collisions at $\sqrt{s} = 8$ TeV", (2013). arXiv:1311.4937. to be published in *Phys. Lett. B*.

[23] CMS Collaboration, "Search for stop in R-parity-violating supersymmetry with three or more leptons and b-tags", *Phys. Rev. Lett.* **111** (2013) arXiv:1306.6643.

[24] CMS Collaboration, "Search for supersymmetry using razor variables in events with b-jets in pp collisions at 8 TeV", CMS Physics Analysis Summary CMS-PAS-SUS-13-004, 2013.

[25] CMS Collaboration, "Search for top squarks decaying to a charm quark and a neutralino in events with a jet and missing transverse momentum", CMS Physics Analysis Summary CMS-PAS-SUS-13-009, 2013.

[26] CMS Collaboration, "Search for top squarks in multijet events with large missing momentum in proton-proton collisions at $\sqrt{s} = 8$ TeV", CMS Physics Analysis Summary CMS-PAS-SUS-13-015, 2013.

[27] CMS Collaboration Collaboration, "Search for stop and higgsino production using diphoton Higgs boson decays", (2013). arXiv:1312.3310. to be published in *Phys. Rev. Lett*.

[28] S. Dimopoulos and G. Giudice, "Naturalness constraints in supersymmetric theories with non-universal soft terms", *Phys. Lett. B* **357** (1995) doi::10.1016/0370-2693(95)00961-J.

[29] CMS Collaboration, "CMS Luminosity Based on Pixel Cluster Counting - Summer 2012 Update", CMS Physics Analysis Summary CMS-PAS-LUM-12-001, 2012.

[30] CMS Collaboration, "The CMS experiment at the CERN LHC", *JINST* **3** (2008) S08004, doi:10.1088/1748-0221/3/08/S08004.

[31] CMS Collaboration, "Particle Flow Event Reconstruction in CMS and Performance for Jets, Taus and MET", CMS Physics Analysis Summary CMS-PAS-PFT-09-001, 2009.

[32] CMS Collaboration, "Commissioning of the Particle-Flow Reconstruction in Minimum-Bias and Jet Events from pp Collisions at 7 TeV", CMS Physics Analysis Summary CMS-PAS-PFT-10-002, 2010.

[33] CMS Collaboration, "Commissioning of the particle-flow event reconstruction with leptons from J/Psi and W decays at 7 TeV", CMS Physics Analysis Summary CMS-PASPFT-10-003, 2010.

[34] M. Cacciari, P. Salam, and G. Soyez, "The anti-kt jet clustering algorithm", *JHEP* **08** (2008) 063, doi:10.1088/1126-6708/2008/04/063.

[35] M. Cacciari, M. Salam, P. Gavin, and G. Soyez, "Pileup subtraction using jet areas", *Phys. Lett. B* **659** (2007) 119, doi:10.1016/j.physletb.2007.09.077, arXiv:0707.1378.

[36] CMS Collaboration, "Determination of Jet Energy Calibration and Transverse Momentum Resolution in CMS", *JINST* **6** (2011) 11002, doi:10.1088/1748-0221/6/11/P11002.

[37] CMS Collaboration, "Performance of muon identification in pp collisions at $\sqrt{s} = 7$ TeV", CMS Physics Analysis Summary CMS-PAS-MUO-10-002, 2010.

[38] CMS Collaboration, "Algorithms for b-Jet identification in CMS", CMS Physics Analysis Summary CMS-PAS-BTV-09-001, 2009.

[39] J. Alwall and et al., "MadGraph/MadEvent v4: the new web generation", *JHEP* **09** (2007) 028, doi:10.1088/1126-6708/2007/09/028.

[40] S. Frixione, P. Nason, and C. Oleari, "Matching NLO QCD computations with Parton Shower simulations: the POWHEG method", *JHEP* **11** (2007) 070, doi:10.1088/1126-6708/2007/11/070.

[41] T. Sjostrand, S. Mrenna, and P. Skands, "PYTHIA 6.4 physics and manual", *JHEP* **05** (2006) doi:10.1088/1126-6708/2006/05/026.

[42] Z. Was, "TAUOLA the library for tau lepton decay", *Nucl. Phys. Proc. Suppl.* **98** (2001) 96, doi:10.1016/S0920-5632(01)01200-2.

[43] GEANT4 Collaboration, "GEANT4a simulation toolkit", *Nucl. Instrum. Meth. A* **506** (2003) 250, doi:10.1016/S0168-9002(03)01368-8.

[44] K. Melnikov and F. Petriello, "Electroweak gauge boson production at hadron colliders through O(alpha(s)**2)", *Phys. Rev. D* **74** (2006) 114017, doi:10.1103/PhysRevD.74.114017, arXiv:hep-ph/0609070.

[45] R. Gavin, Y. Li, F. Petriello, and S. Quackenbush, "W Physics at the LHC with FEWZ 2.1", *Comput. Phys. Commun.* **184** (2013) 208–214, doi:10.1016/j.cpc.2012.09.005, arXiv:1201.5896.

[46] N. Kidonakis, "Next-to-next-to-leading-order collinear and soft gluon corrections for t-channel single top quark production", *Phys. Rev. D* **83** (2011) 091503, doi:10.1103/PhysRevD.83.091503, arXiv:1103.2792.

[47] N. Kidonakis, "NNLL resummation for s-channel single top quark production", *Phys. Rev. D* **81** (2010) 054028, doi:10.1103/PhysRevD.81.054028, arXiv:1001.5034.

[48] N. Kidonakis, "Two-loop soft anomalous dimensions for single top quark associated production with a W- or H-", *Phys. Rev. D* **82** (2010) 054018, doi:10.1103/PhysRevD.82.054018, arXiv:1005.4451.

[49] N. Kidonakis, "Next-to-next-to-leading soft-gluon corrections for the top quark cross section and transverse momentum distribution", *Phys. Rev. D* **82** (2010) 114030, doi:10.1103/PhysRevD.82.114030, arXiv:1009.4935.

[50] N. Kidonakis, "Differential and total cross sections for top pair and single top production", doi:10.3204/DESY-PROC-2012-02/251, arXiv:1205.3453.

[51] M. Garzelli, A. Kardos, C. Papadopoulos, and Z. Trocsanyi, "t $\bar{t}$ W^{+-} and t $\bar{t}$ Z Hadroproduction at NLO accuracy in QCD with Parton Shower and Hadronization effects", *JHEP* **1211** (2012) 056, doi:10.1007/JHEP11(2012)056, arXiv:1208.2665.

[52] J. M. Campbell and R. Ellis, "MCFM for the Tevatron and the LHC", *Nucl. Phys. Proc. Suppl.* **205-206** (2010) 10–15, doi:10.1016/j.nuclphysbps.2010.08.011, arXiv:1007.3492.

[53] R. Field, "Early LHC Underlying Event Data - Findings and Surprises", technical report.

[54] J. Pumplin and et al, "New generation of parton distributions with uncertainties from global QCD analysis", *JHEP* **07** (2002) 012, doi:10.1088/1126-6708/2002/07/012.

[55] D. Tovey, "Supersymmetric particle mass measurement with boost-corrected constransverse mass", *JHEP* **03** (2010) doi:10.1007/JHEP03(2010)030.

[56] G. Polesello and D. Tovey, "On measuring the masses of pair-produced semi-invisibly decaying particles at hadron colliders", *JHEP* **04** (2008) doi:10.1088/1126-6708/2008/04/034.

[57] CMS Collaboration, "Missing transverse energy performance of the CMS detector", *JINST* **6** (2011) P091001, doi:10.1088/1748-0221/6/09/P09001.

[58] CMS Collaboration, "Performance of Missing Transverse Momentum Reconstruction Algorithms in Proton-Proton Collisions at s = 8 TeV with the CMS Detector", CMS Physics Analysis Summary CMS-PAS-JME-12-002, 2012.

[59] S. Malik and G. Watt, "Ratios of W and Z cross sections at large boson p_T as a constraint on PDFs and background to new physics", *JHEP* **1402** (2014) 025, doi:10.1007/JHEP02(2014)025.

[60] CMS Collaboration, "Interpretation of searches for supersymmetry with simplified models", *Phys. Rev. D* **88** (2013) 052017, doi:10.1103/PhysRevD.88.052017.

[61] J. Alwall, P. Schuster, and N. Toro, "Simplified Models for a First Characterization of New Physics at the LHC", *Phys. Rev. D* **79** (2009) doi:10.1103/PhysRevD.79.075020.

[62] J. Alwall, M. Le, and M. Lisanti, "Model-Independent Jets plus Missing Energy Searches", *Phys. Rev. D* **79** (2009) doi:10.1103/PhysRevD.79.015005.

[63] D. Alves, N. Arkani-Hamed, and S. Arora, "Simplified Models for LHC New Physics Searches", *J. Phys. G: Nucl. Part. Phys.* **39** (2012) 105005, doi:10.1088/0954-3899/39/10/105005.

[64] A. Read, "Presentation of search results: the CL s technique", *J. Phys. G* **28** (2002) 2693, doi:10.1088/0954-3899/28/10/313.

[65] T. Junk, "Confidence level computation for combining searches with small statistics", *Nucl. Instr. and Meth. A* **434** (1999) 435, doi:10.1016/S0168-9002(99)00498-2.

[66] CMS Collaboration, "CMS Luminosity Based on Pixel Cluster Counting - Summer 2013 Update", CMS Physics Analysis Summary CMS-PAS-LUM-13-001, 2013.

[67] A. Kulesza and L. Motyka, "Threshold resummation for squark-antisquark and 645 gluino-pair production at the LHC", *Phys. Rev. Lett.* **102** (2009) 111802, doi:doi:10.1103/PhysRevLett.102.111802.

[68] A. Kulesza and L. Motyka, "Soft gluon resummation for the production of gluino-gluino and squark-antisquark pairs at the LHC", *Phys. Rev. Lett.* **80** (2009) 095004, doi:doi:10.1103/PhysRevLett.80.095004.

[69] W. Beenakker and et al., "Soft-gluon resummation for squark and gluino hadroproduction", *JHEP* **12** (2009) 041, doi:doi:10.1088/1126-6708/2009/12/041.

[70] W. Beenakker and et al., "Squark and gluino hadroproduction", *Int. J. Mod. Phys. A* **26** (2011) 2637, doi:doi:10.1142/S0217751X11053560.

[71] M. Kramer and et al., "Supersymmetry production cross sections in pp collisions at sqrts = 7 TeV", (2012). arXiv:1206.2892.

[72] M. Botje and et al, "The PDF4LHC Working Group Interim Recommendations", arXiv:1101.0538.